# Radiation-Stability of Smectite

**ARTICLE** *in* ENVIRONMENTAL SCIENCE AND TECHNOLOGY · DECEMBER 2008

Impact Factor: 5.33 · DOI: 10.1021/es800766b · Source: PubMed



**7 AUTHORS**, INCLUDING:

Stéphanie Sorieul
French National Centre for Scientific Resea…
**27** PUBLICATIONS **316** CITATIONS
SEE PROFILE

Thierry Allard
French National Centre for Scientific Resea…
**88** PUBLICATIONS **1,171** CITATIONS
SEE PROFILE

# Radiation-Stability of Smectite

STÉPHANIE SORIEUL,[*,†,#] THIERRY ALLARD,[‡] LUMIN M. WANG,[§] CAROLINE GRAMBIN-LAPEYRE,[||] JIE LIAN,[⊥] GEORGES CALAS,[‡] AND RODNEY C. EWING[§,⊥]

*Laboratoire Pierre Süe, UMR 9956 CEA-CNRS, 91191 Gif/Yvette cedex, France, Institut de Minéralogie et de Physique des Milieux Condensés, UMR 7590, Université Paris 6 et 7, IPGP, 140 rue de Lourmel, 75015 Paris, France, Department of Nuclear Engineering and Radiological Sciences, Cooley Building, 2355 Bonisteel Boulevard, University of Michigan, Ann Arbor, Michigan 48109-2104, Centre de Géologie de l'Ingénieur, Université de Marne-la-Vallée, Cité Descartes - Bâtiment IFI, 5, Boulevard Descartes, 77454 Marne-la-Vallée cedex 2, France, and Department of Geological Sciences, C.C. Little Building, University of Michigan, Ann Arbor, Michigan 48109-1005*

*Received March 17, 2008. Revised manuscript received August 29, 2008. Accepted September 1, 2008.*

The safety assessment of geological repositories for high-level nuclear waste and spent nuclear fuel requires an understanding of the response of materials to high temperatures and intense radiation fields. Clays, such as smectite, have been proposed as backfill material around waste packages, but their response to intense radiation from short-lived fission products and alpha decay of sorbed actinides remains poorly understood. Cumulative doses may amorphize clays and may alter their properties of sorption, swelling, or water retention. We describe the amorphization of smectites induced by electron and heavy ion irradiations to simulate ionizing radiation and alpha recoil nuclei, respectively. A new "bell-shaped" evolution of the amorphization dose with temperature has been determined. The maximum dose for amorphization occurs at about 300−400 °C, showing that temperature-induced dehydroxylation enhances amorphization. The exact shape of the bell-shaped curves depends on the interlayer cation. At ambient temperature, ionizing radiation and alpha-decay events do not show the same efficiency. The former results in amorphization at doses between $10^{10}$−$10^{11}$ Gy which are greater than the total radiation dose expected for radioactive waste over $10^6$ years. In contrast, alpha-decay events amorphize clays at doses as low as 0.13−0.16 displacements per atom, i.e. doses consistent with nuclear waste accumulated over approximately 1000 yrs. However, the limited penetration of alpha particles and recoil nuclei, in the 100 nm - 20 $\mu$m range, will minimize damage. Clays will not be amorphized unless the waste package is breached and released actinides are heavily sorbed onto the clay overpack.

## Introduction

The radiation-induced crystalline to amorphous transition of minerals has received considerable attention in the past decade with the aim to establish scientific basis for selecting radiation-resistant materials for the disposal and isolation of radioactive waste (*1*−*3*). Realistic models used for the long-term prediction of radionuclide transport have to take into account radiation damage in containment materials, as a specific aftermath of radioactive waste (*4*). Experimental investigations of various ceramics and natural minerals have highlighted the role of structure and composition on the stability under irradiation (*5, 6*).

Radiation-induced amorphization may affect the stability of materials, resulting in significant changes of important physical and chemical properties such as for zeolites, in which amorphization alters sorption properties (*7, 8*). This may also have important implications for clay minerals such as smectites that are considered as efficient barriers against radionuclide migration in nuclear waste disposals (*9, 10*). In several concepts of waste disposal mainly in Japan and various European countries, smectites are major components either of the geological host rock or the engineered barrier surrounding the radioactive waste. In the engineered barriers, severe irradiation and ultimately amorphization may result from the alpha decay of long-lived actinides (e.g., $^{237}$Np) and the ionizing radiation of fission products (e.g., $^{137}$Cs and $^{90}$Sr). The most important properties of smectites, which may be influenced by irradiation, include water retention, swelling or cation exchange capacity. Solubility as well may be altered as previously observed on other silicates minerals through experimental irradiations (*11, 12*).

Thus, it is necessary to determine the radiation parameters under which clays may become amorphous. However despite its environmental importance, this issue is poorly documented. An early study of MX80 smectite exchanged with short-lived alpha emitters has shown amorphization for $5 \times 10^{18}$ alpha event per gram of clay (*10*). Corresponding doses for 5 MeV alpha particles (ionizing particles) and 100 keV recoil nuclei (displacive atoms) can be estimated at 4 GGy and 0.2 displacements per atom (dpa), respectively. Other study also evidenced morphological changes in clay minerals exchanged with an alpha-radiation source (*13*). Electron-irradiation of smectites showed that the amorphization dose evolves as a "bell-shaped" curve as a function of temperature with a maximum amorphization dose around 300−400 °C, which so far appears unique when compared to other investigated materials (*7, 14*). The increasing part of the curve was related to the decreasing involvement of radiolytic products of hydration water together with interlayer cation immobility. The decreasing part was associated to dehydroxylation of the clay structure. Furthermore, the amorphization dose at room temperature was $3 \times 10^{10}$ Gy for a $K^+$-exchanged montmorillonite.

The present study investigates the temperature-dependent conditions for amorphization under heavy-ion and electron beams, simulating alpha-recoil nucleus and ionizing radiation, respectively. The potential effect of the chemical environment of smectites is investigated on a reference montmorillonite by using different interlayer cations having contrasting hydration energies ($Ca^{2+}$, $Na^+$, $Li^+$, and $K^+$).

* Corresponding author phone: 33 5 57 12 08 46; fax: 33 5 57 12 08 01; e-mail: sorieul@cenbg.in2p3.fr.
† UMR 9956 CEA-CNRS.
‡ Université Paris 6 et 7.
§ Department of Nuclear Engineering and Radiological Sciences, University of Michigan.
|| Université de Marne-la-Vallée.
⊥ Department of Geological Sciences, University of Michigan.
# Current address: Center d'Etudes Nucleaires de Bordeaux-Gradignan, UMR 5797, Le Haut-Vigneau BP120, 33175 Gradignan Cedex, France.

10.1021/es800766b CCC: $40.75 
Published on Web 10/16/2008

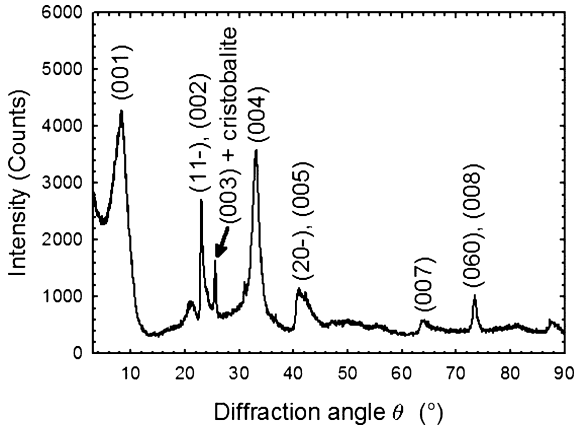


**FIGURE 1. X-rays diffraction pattern for the $Na^+$-montmorillonite (0.5 $\mu$m fraction) after extraction and purification processes. Main diffraction peaks are assigned to the corresponding crystallographic position. The (001) peak corresponds to a distance $d = 12,2$ Å.**

## Experimental Section

**Montmorillonite Purification.** Smectites are hydrous clay minerals which expand upon contact with water and reversibly exchange cations from solution. Their structure consists of two tetrahedral layers with Si-containing sites surrounding one octahedral layer with typically Al, Mg composition. In the present study, we used a montmorillonite, which is a subgroup of smectites with charges of 0.2−0.6 per half-unit-cell, and a dioctahedral structure where one of every three octahedral positions is vacant. Heterovalent substitutions in octahedral (e.g., $Mg^{2+}$, $Fe^{2+}$ for $Al^{3+}$) and tetrahedral ($Al^{3+}$ for $Si^{4+}$) sites induce a charge deficiency, which is balanced by exchangeable cations in interlayer position. These cations are typically surrounded by water molecules. The general formula is $M_x^+(Al_{4-x}Mg_x)(Si_{8.0})O_{20}(OH)_4$, where $M^+$ is an interlayer cation and x is the layer charge. The structure and layer charge of montmorillonites are at the origin of many of their physicochemical properties including cation exchange, water retention and swelling. The investigated sample was extracted from the Wyoming bentonite MX-80, a widely used montmorillonite-rich clay reference for studies dealing with backfill material (see e.g. ref *15* for mineral components). A size fraction below 0.5 $\mu$m was prepared by centrifugation, allowing the separation of the clay from associated minerals including quartz and feldspars. Ancillary iron oxides were removed with citrate-dithionite bicarbonate (DCB) treatment (*16*). Removal of carbonates was performed with acetic buffer (pH = 5). Both DCB and acetic treatments were performed at 80 °C. The resulting montmorillonite samples were lithium-, sodium-, potassium-, and calcium-exchanged by stirring the clay in 1 mol.$L^{-1}$ of chloride solution during 6 h, this treatment was repeated once more time. The excess salts were removed by repeated washing (five consecutive washing treatments) with deionized water. The chloride concentration was checked with the silver ions test ($AgNO_3$). Purity of samples was checked by X-ray diffraction and Fourier transform infrared spectroscopy. Figure 1 presents the X-rays diffraction pattern of the purified sample exchanged with $Na^+$ ions.

**Chemical Composition of the Montmorillonite.** The chemical analyses of the clays were performed by inductively coupled plasma - atomic emission spectroscopy at the CRPG (Nancy, France). The average composition is (e.g., for the K-exchanged sample)

$K_{0.70}Na_{0.07}(Si_{7.72}\ Al_{0.28})(Al_{3.10}Mg_{0.47}FeIII_{0.31}FeII_{0.05})Ti_{0.01}O_{20}(OH)_4$

Mineralogical composition of each purified sample is reported in Table 1.

**Irradiation of Clay.** Samples were prepared by wet deposition on a 3 mm holey carbon film supported by a copper grid. A heating stage was used for both experiments to examine the temperature effect on irradiation damage. Radiation damages under 200 keV electron beam were observed *in situ* using a JEOL 2010 F transmission electron microscope. The electron flux was determined based on the current density on the image screen with the electron beam aligned through a hole in the sample. The temperature dependence of amorphization doses was measured over a range of 25−600 °C. Amorphization doses were measured at the same dose rate of $4.75 \times 10^{18}$ e-/($cm^2$.s) for 25−350 °C and of $8 \times 10^{18}$ e-/($cm^2$.s) for 400−600 °C, corresponding to the classical methodology for minerals and ceramics (*17*). The details of the calculation of doses, using Bethe equation, are described elsewhere (*18*). Ion beam irradiations and *in situ* TEM observations were performed using the HVEM-Tandem facility at the Argonne National Laboratory (USA). Samples were irradiated by 1 MeV $Kr^+$ from ambient temperature to 500 °C. The ion flux was $3 \times 10^{11}$ ions/($cm^2$.s). The electron microscope was operated at 300 keV for the *in situ* observations. In the case of heavy ions, SRIM2003 calculations were performed in full cascades mode to calculate the electronic and nuclear energy deposition and the number of displacements per atom (dpa) (*19*). The displacement energy being unknown for montmorillonites, the default value in SRIM was used (20 eV) for all elements in the minerals. In both experiments, the amorphization process was monitored by selected area electron diffraction during TEM observations. To separate the effects of ion irradiation from that of electron irradiation, the electron beam was only intermittently turned on for the purpose observation.

**TGA Analysis.** Thermogravimetric analysis (TGA) was performed on about 100 mg, operating at 2.5 °C/min from ambient temperature to 800 °C in an argon atmosphere. The inert atmosphere prevented the samples from oxidation during thermal treatment. Derivative TGA diagrams were used to enhance the dehydration and dehydroxylation steps.

## Results and Discussion

**Thermal Behavior of Reference Samples.** Dehydration occurs in a range of 60−120 °C according to the loss of adsorbed water (not shown). The major dehydration thresholds, identified as the initial water contents in Table 2, decrease in the order $Ca^{2+} > Li^+ > Na^+ > K^+$, in accordance with the relative hydration energies of cations as seen from ionic potentials (Table 2). As a matter of fact, a higher ionic potential corresponds to higher dehydration temperature of montmorillonites (*20*). Figure 2 presents the derivative of TGA in the 200−800 °C range. A small weight loss at a percent level or less is first observed around 300−400 °C for $Na^+$, $Ca^{2+}$ and weakly for $Li^+$, $K^+$. The corresponding temperatures increase in the sequence $Ca^{2+} < Na^+ < K^+ < Li^+$. These features are tentatively assigned to incipient dehydroxylation. A strong, major dehydroxylation step follows in the range 600 °C-650 °C with characteristic temperatures decreasing in the sequence $Ca^{2+} > Na^+ > K^+ > Li^+$. It does not correspond to an ordered sequence of ionic charge nor ionic potential (Table 2). However these results show that the nature of interlayer cation strongly influences the temperature of structural water loss which is a known behavior for montmorillonites (*21, 22*).

**Temperature Dependence of Amorphization Induced by Electrons and Heavy Ions.** The progressive change from crystalline to aperiodic state under irradiation was followed under electron diffraction patterns as illustrated at 300 °C on the $Na^+$-smectite (Figure 3). Selected area electron diffraction patterns show the initial spots arising from smectite structure (Figure 3a). As the cumulative dose increases, these spots loose intensity to the benefit of diffuse rings resulting from

**TABLE 1. Chemical Composition (%) of Purified Fraction for $Li^+$-, $Na^+$-, $K^+$-, and $Ca^{2+}$-Montmorillonites**

| cation | $SiO_2$ | $Al_2O_3$ | MgO | $Fe_2O_3$ | $Na_2O$ | CaO | $K_2O$ | $Li_2O$ | $TiO_2$ | PF | total | FeO |
|---|---|---|---|---|---|---|---|---|---|---|---|---|
| Li | 59.99 | 22.53 | 2.23 | 3.62 | 0.11 | - - | - - | 1.00 | 0.10 | 12.96 | 99.54 | 0.50 |
| Na | 56.54 | 19.81 | 3.91 | 1.27 | 2.99 | 0.12 | 0.16 | - - | 0.06 | 15.35 | 100.21 | 0.31 |
| K | 59.08 | 21.80 | 2.31 | 3.68 | 0.30 | - - | 4.14 | - - | 0.09 | 8.23 | 99.63 | 0.50 |
| Ca | 56.51 | 21.38 | 2.23 | 3.53 | 0.08 | 2.70 | - - | - - | 0.10 | 12.87 | 99.40 | 0.60 |

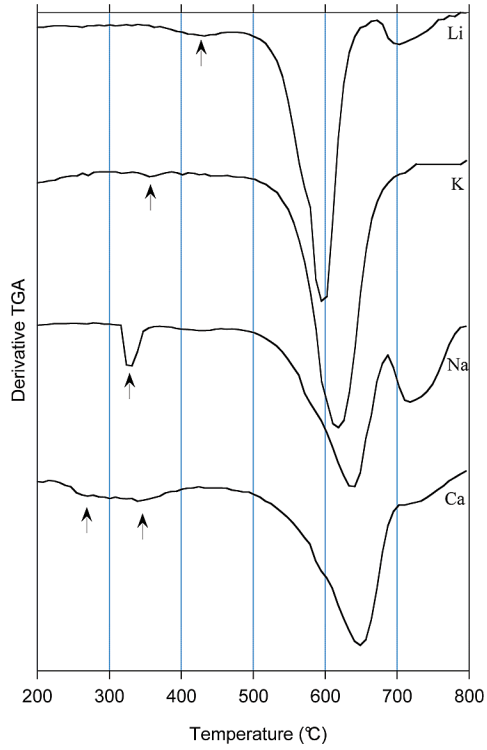


**FIGURE 2. Derivative of thermogravimetric analysis for $Li^+$-, $K^+$-, $Na^+$-, and $Ca^{2+}$-exchanged montmorillonites in the region 300−700 °C. Arrows indicate small thresholds of water loss anticipating dehydroxylation thresholds and tentatively assigned to incipient dehydroxylation.**

radiation-induced amorphous structure (Figure 3c). The situation in-between corresponds to incomplete amorphization (Figure 3b). When all the analyzed area is amorphous, i.e. only broad diffuse rings are visible, the amorphization dose is determined. Amorphization dose was determined in several parts of each sample in order to minimize the error on the measurements.

Resulting amorphization curves related to $Li^+$-, $Na^+$-, $K^+$-, and $Ca^{2+}$-montmorillonites as a function of temperature are presented in Figures 4 and 5. The amorphization doses are reported in Table 3. For all samples the dose increases with the temperature, reaches a maximum around 350−400 °C and subsequently decreases, thus describing a "bell-shaped" curve. This confirms data of Gu et al. (*7*) obtained for the amorphization of a $K^+$-montmorillonite. The maximum amorphization doses are in the range $2-3 \times 10^{12}$ Gy for electrons and around 0.15−0.20 dpa for $Kr^+$ ions. However, errors on measurement make bell-shaped curves for K and Ca much less obvious than for other cations. This may suggest a better radiation resistance which may be related to the lower mobility of the cations with increasing temperature.

This temperature dependence of the amorphization dose appears different in smectites from that in other materials, which show monotonous increasing (various minerals and ceramics) or decreasing (zeolites) dependences with temperature (*23*). The amorphization curve for smectites can be explained by two main processes: (i) As in ceramics, the amorphization dose increases with temperature because thermal annealing of defects competes with damage accumulation (*23*): the higher the temperature, the more efficient the annealing. In the temperature range of the rising amorphization curve, the smectite is thermally stable and progressively loses hydration water. (ii) By contrast the decreasing part of the amorphization curve in smectites implies an increasing sensitivity to structure breakdown with temperature. By analogy to zeolites (*16*) this might be related to the combining effect of irradiation damage and thermal destabilization of the structure as in K-montmorillonites (*7*). As a matter of fact, montmorillonites are thermally amorphized from 700 °C but may be progressively dehydroxylated from lower temperatures. Dehydroxylation is directly related to the thermal breakdown of the smectite structure.

Consequently, montmorillonite is confirmed to exhibit two successive radiation-induced amorphization regimes as a function of temperature: an annealing regime forcing the amorphization dose to increase and a dehydroxylation regime inducing a decreasing trend whatever the irradiation. It is proposed that incipient dehydroxylation would control the change between the two processes responsible for the "bell-shaped" curve. Despite similar "bell-shaped" curves, the processes of radiation-induced damage are different between electron and heavy ions. The energy transferred to the nucleus of target atoms by electron irradiation is too small to produce significant structural damage directly. Thus, the electron damage is mainly due to ionization, amorphization occurring through the so-called radiolysis process (*24*). By opposition, ion irradiation produces damage by both ionization and nuclear collision.

**Influence of the Interlayer Cation on Smectite Amorphization.** The amorphization curves shift among the samples suggesting the role of interlayer cations on the

**TABLE 2. Ionic Potential, Initial Water Content Percent, Dehydroxylation Temperature, Dehydroxylation Threshold Temperature, and Amorphization Temperature $T_{Dmax}$ for $Li^+$-, $Na^+$-, $K^+$-, and $Ca^{2+}$-Montmorillonites[a]**

| cation | ionic potential(r/ion charge) | initial $H_2O$ hydration % | dehydroxyl. T (°C) | dehydroxyl. threshold T (°C) | amorphization $T_{Dmax}$ (°C) |
|---|---|---|---|---|---|
| Li | 1.11 | 6.6 | 600 | 425 | 450/420 |
| K | 0.66 | 3.4 | 620 | 360 | 455/390 |
| Na | 0.86 | 4.6 | 640 | 330 | 350/345 |
| Ca | 1.75 | 9.1 | 650 | 270−345 | 350/350 |

[a] Initial water content and dehydroxylation temperatures are determined with ATD/ATG. $T_{Dmax}$ is the temperature for maximum amorphization dose fitted with a cubic spline function for electron and krypton irradiations, respectively.

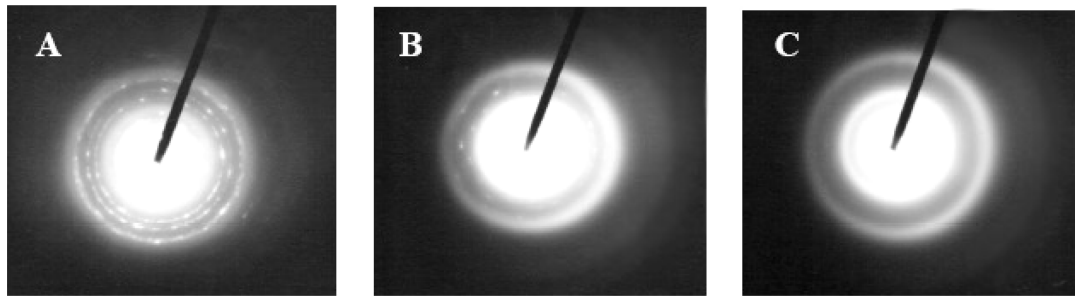


**FIGURE 3. Selected area electron diffraction patterns of $Na^+$-smectite as a function of irradiation dose with 200 keV electron beam at 300 °C: (A) low dose, 420 GGy; (B) medium dose, 750 GGy; and (C) amorphization dose 1995 GGy.**

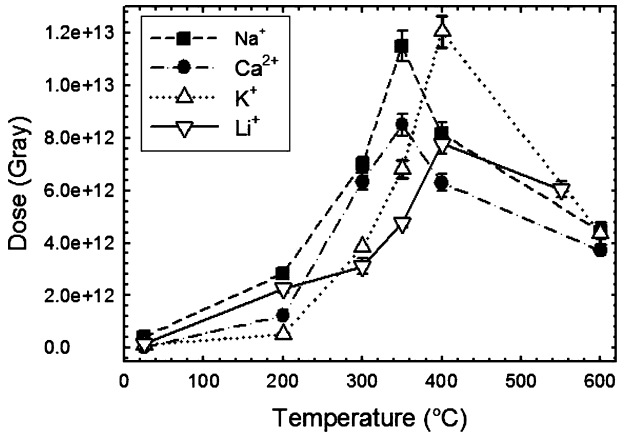


**FIGURE 4. Amorphization dose curves for $Li^+$- $Na^+$-, $K^+$-, and $Ca^{2+}$-montmorillonites irradiated with electrons as a function of temperature.**

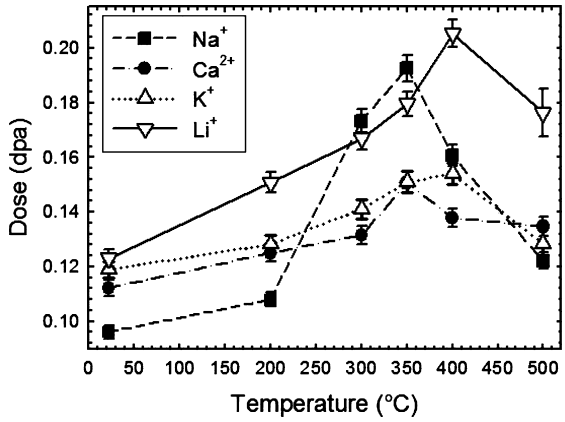


**FIGURE 5. Amorphization dose curves for $Li^+$-, $Na^+$-, $K^+$-, and $Ca^{2+}$-montmorillonites irradiated with $Kr^+$ ions as a function of temperature.**

crystalline to aperiodic transition. This trend is similar for both electron and $Kr^+$ ion irradiation experiments (Figure 4 and 5).

In the low temperature range (0−300 °C), no significant differences between the samples is observed despite the strong differences in the initial water content (Table 2). The influence of interlayer water on amorphization, as previously proposed (*7*), should result in amorphization doses increasing in the order $Ca^{2+}$, $Li^+$, $Na^+$, $K^+$ at a given temperature. Such an effect is not observed, indicating that the role of interlayer water in assisting the amorphization process cannot be confirmed from our experiments.

The major difference between samples arises from a significant shift of the temperature of maximum amorphization dose, hereafter referred to as $T_{Dmax}$. Thus, $T_{Dmax}$ for $Li^+$- and $K^+$-montmorillonites is around 400 °C, whereas it is around 350 °C for $Na^+$ and $Ca^{2+}$ clays. The present results are in agreement with a previous experiment on $K^+$-montmorillonite (*7*), showing a $T_{Dmax}$ in the range 375−400 °C. Experimental data fit with cubic splines gives a sequence of $T_{Dmax}$ in the order $Li^+ > K^+ > Ca^{2+} > Na^+$ (Table 2).

Obviously, the $T_{Dmax}$ parameter is not related to the hydration energy or ionic potential of cations, as evidenced in Table 2. Instead, smectite amorphization temperature seems to be inversely related to the beginning temperature of dehydroxylation. Indeed, the analysis of the TGA curves shows that dehydroxylation starts earlier for Na and Ca cations than for K and Li cations, as seen in Table 2. This phenomenological relationship is consistent with the specific physicochemical properties of the cations, i.e. $Li^+$, $K^+$ versus $Ca^{2+}$, $Na^+$. Dehydration induces irreversible lithium migration into an octahedral sheet beyond 200 °C, giving rise to the well-known Hofmann-Klemen effect (*25, 26*). This small cation is able to migrate and locate close to the sites of heterovalent substitution within the layer (e.g., close to $Mg^{2+}$). As a result, the local charge balance is restored, producing a more neutral layer. Besides, layers of $K^+$-montmorillonites collapse during dehydration for relatively low temperatures and give an anhydrous structure close to those of micas (*27*). Accordingly, the dehydroxylation of mica occurs at higher temperature than smectite (*28*). As a result, in the absence of interlayer water, stronger $K^+$-layer interactions and more stable charge compensation are expected. These characteristics would result in slightly enhanced stability under electron or ion beam of Li- and K-montmorillonites with respect to $Na^+$ and $Ca^{2+}$ interlayer cations. However, the behavior of

**TABLE 3. Irradiation Parameters for Electrons and $Kr^+$ Ions at Room Temperature[a]**

| | electrons | | | $Kr^+$ ions | | | |
|---|---|---|---|---|---|---|---|
| | Da (gray) | (dE/dx)e (MeV/cm) | displ. dose (dpa) | Da (gray) | (dE/dx)e (MeV/cm) | (dE/dx)n (MeV/cm) | displ. dose (dpa) |
| Na | $4.2 \times 10^{11}$ | 14.96 | $6.2 \times 10^{-3}$ | $5.3 \times 10^{7}$ | 9144 | 4050 | 0.128 |
| Ca | $2.4 \times 10^{10}$ | 14.29 | $3.8 \times 10^{-4}$ | $6.2 \times 10^{7}$ | 9112 | 4084 | 0.152 |
| K | $1.6 \times 10^{11}$ | 14.06 | $2.5 \times 10^{-3}$ | $6.1 \times 10^{7}$ | 9028 | 4125 | 0.161 |
| Li | $1.3 \times 10^{11}$ | 14.49 | $2.1 \times 10^{-3}$ | $6.8 \times 10^{7}$ | 9158 | 4147 | 0.165 |

[a] $D_a$: ionization dose of amorphization at room temperature; $(dE/dx)_e$: electronic stopping power; $(dE/dx)_n$: nuclear stopping power; dpa: displacement per atom.

$Li^+$- and $K^+$-montmorillonites cannot be distinguished owing to the lack of data between 400 and 550 °C.

**Amorphization at Ambient Temperature: The Long-Term Relevance.** Amorphization at ambient temperature is relevant to the long-term performance of the engineered barrier. After an initial hot period (around 150 °C), the average dominant temperature of the clay during the waste disposal existence will be ambient temperature. The amorphization doses at room temperature are around $10^{11}$ Gy and 0.128−0.165 dpa for electron and heavy ions, respectively. In the case of electron irradiation, the dose is 1 order of magnitude above the one measured for the $K^+$-exchanged Arizona montmorillonite by Gu et al. (*7*).

The amorphization doses determined in this study may be compared to the cumulative doses estimated in high level nuclear waste repositories (*2, 29*). For electron irradiation, values of $10^{11}$ Gy are high as compared with the $10^{10}$ Gy level expected to accumulate over $10^6$ years, a period of concern for nuclear waste repositories. Thus, it is unlikely that the exposure of the clay backfill to ionizing sources will be sufficiently high to amorphize clay and change its properties. In addition, the low dose rate expected in a geological repository may result in enhanced defect annealing. By contrast, doses resulting from ballistic interactions (heavy ions) are comparable to those that may be reached in the event the waste package is breached and alpha-emitters are released and sorbed directly onto the surface of the clay. With the assumption that alpha events in the waste (*30*) are transferred to the clay, amorphization (at 0.1−0.2 dpa) occurs after about 1000 years for an integrated activity of $1.5 \times 10^{19}$ events/$cm^3$. This result is similar to a previous estimation derived from experimental loading of clay with alpha emitters (*9*). It is also close to the duration required for amorphization of a ceramics from nuclear waste (*31*). However, the dose rate of the irradiation experiments is at least 4−8 orders of magnitude higher than the dose rate expected in most radioactive repositories (*2*). Thus, the interpretation of the experimental results represents a worst case scenario in which long-term annealing under ambient conditions has not been considered.

## Acknowledgments

This work was supported by a joint NSF-CNRS program. S. Sorieul's PhD program was supported by ANDRA. N. Michau is acknowledged for scientific coordination at ANDRA, France. This is an IPGP contribution N°2409.

## Literature Cited

(1) Hobbs, L. W.; Clinard, F. W. J.; Zinkle, S. J.; Ewing, R. C. Radiation effects in ceramics. *J. Nucl. Mater.* **1994**, *216*, 291–321.
(2) Ewing, R. C.; Weber, W. J.; Clinard, F. W. J. Radiation effects in nuclear waste forms for high-level radioactive waste. *Progress in Nuclear Energy* **1995**, *29* (2), 63–127.
(3) Dran, J.-C. Radiation effects in radioactive waste storage materials. *Solid State Phenomena* **1993**, *30/31*, 367–378.
(4) Weber, W. J.; Ewing, R. C.; Meldrum, A. The kinetics of alpha-decay-induced amorphization in zircon and apatite containing weapons-grade plutonium or other actinides. *J. Nucl. Mater.* **1997**, *250*, 147–155.
(5) Meldrum, A.; Boatner, L. A.; Ewing, R. C. Displacive radiation effects in the monazite- and zircon-structure orthophosphates. *Phys. Rev. B* **1997**, *56*, 13805–13814.
(6) Wang, L. M.; Ewing, R. C. Ion beam induced amorphization of complex ceramic materials-minerals. *MRS Bull.* **1992**, *17* (5), 38–44.
(7) Gu, B. X.; Wang, L. M.; Minc, L. D.; Ewing, R. C. Temperature effects on the radiation stability and ion exchange capacity of smectites. *J. Nucl. Mater.* **2001**, *297*, 345–354.
(8) Wang, L. M.; Chen, J.; Ewing, R. C. Radiation and thermal effects on porous and layer structured materials as getters of radionuclides. *Cur. Opin. Solid State Mater. Sci.* **2004**, *8*, 405–418.
(9) Pusch, R. *Waste Disposal in Rock. Elsevier*, Amsterdam, 1994; p 490.
(10) Meunier, A.; Velde, B.; Griffault, L. The reactivity of bentonites: a review. An application to clay barrier stability for nuclear waste storage. *Clay Miner.* **1998**, *33*, 187–196.
(11) Petit, J. C.; Dran, J.-C.; Della Mea, G. Effects of ion implantation on the dissolution of minerals. Part II. Selective dissolution. *Bull. Mineral.* **1987**, *110*, 25–42.
(12) Weber, W. J.; Ewing, R. C.; Catlow, C. R. A.; Diaz de la Rubia, T.; Hobbs, L. W.; Kinoshita, C.; Matzke, H.; Motta, A. T.; Nastazi, M.; Salje, E. H. K.; Vance, E. R.; Zinkle, S. J. Radiation effects in crystalline ceramics for the immobilization of high-level nuclear waste and plutonium. *J. Mater. Res.* **1998**, *13* (6), 1434–1484.
(13) Haire, R. G.; Beall, G. W., *Consequences of radiation from sorbed transplutonium elements on clays selected for waste isolation. In Radioactive Waste in Geologic Storage; ACS Symposium Series 100*; Gould, R. F., Ed; Miami Beach, Florida. 11−15 Sept., 1978; p 291−295.
(14) Wang, L. M.; Wang, S. X.; Gong, W. L.; Ewing, R. C. Temperature dependence of Kr ion-induced amorphization of mica minerals. *Nucl. Instr. Meth. Phys. Res. B* **1998**, *141*, 501–508.
(15) Guillaume, D.; Neaman, A.; Cathelineau, M.; Mosser-Ruck, R.; Peiffert, C.; Abdelmoula, M.; Dubessy, J.; Villieras, F.; Baronnet, A.; Michau, N. Experimental synthesis of chlorite from smectite at 300°C in the presence of metallic Fe. *Clay Miner.* **2003**, *38*, 281–302.
(16) Mehra, O. P.; Jackson, M. L., *Iron oxide removal from soils and clays by a dithionite-citrate system buffered with sodium bicarbonate. In Clays and Clay Minerals*, Swineford, A., Ed.; Pergamon Press, London, 1960; pp 317−327.
(17) Wang, S. X.; Wang, L. M.; Ewing, R. C. Electron and ion irradiation of zeolites. *J. Nucl. Mater.* **2000**, *278*, 233–241.
(18) Utsunomiya, S.; Wang, L. M.; Douglas, M.; Clark, S. B.; Ewing, R. C. The effect of ionizing radiation on uranophane. *Am. Mineral.* **2003**, *88*, 159.
(19) Ziegler, J. F.; Biersack, J. P.; Littmark, U. *The Stopping and Range of Ions in Solids*;Pergamon: New York, 1985.
(20) Zabat, M.; Van Damme, H. Evaluation of the energy barrier for dehydration of homoionic (Li, Na, Cs, Mg, Ca, Ba, Alx(OH)z+y and La)-montmorillonite by a differentiation method. *Clay Miner.* **2000**, *35*, 357–363.
(21) Mackenzie, R. C.; Bishui, B. M. The montmorillonite differential thermal curve. *Clay Min. Bull.* **1958**, *3*, 276.
(22) El-Akkad, T. M.; Flex, N. S.; Guindy, N. M.; El-Massry, S. R.; Nashed, S. Thermal analyses of mono- and divalent montmorillonite cationic derivatives. *Thermochim. Acta* **1982**, *59*, 9–17.
(23) Ewing, R. C.; Meldrum, A.; Wang, L. M., Wang, S., *Radiation-induced amorphization. In Transformation Processes in Minerals*; Redfern, S. A. T.; Carpenter, M. A., Eds.; Mineralogical Society of America., 2000; Vol. 39, pp 319−361.
(24) Hobbs, L. W.; Pascucci, M. R. *J. Phys. (Paris)* **1980**, *C6*, 237.
(25) Hofmann, U.; Klemen, R. Verlust der Austauschfähigkeit von Lithiumionen an Bentonit durch Erhitzung. *Zeitschrift Anorganische Chemie* **1950**, *262*, 95–99.
(26) Madejova, J.; Bujdak, J.; Petit, S.; Komadel, P. Effects of chemical composition and temperature of heating on the infrared spectra of Li-saturated dioctahedral smectites. (II) Near-infrared region. *Clay Miner.* **2000**, *35*, 753–761.
(27) Brindley, G. W.; Brown, G. *Crystal Structures of Clay Minerals and their X-ray Identification.* Mineralogical Society: London, 1980; p 495.
(28) Brigatti, M. F.; Guggenheim, S. *Mica Crystal chemistry and the influence of pressure, temperature, and solid solution on atomistic models. In Micas: Crystal Chemistry and Metamorphic Petrology*; Mottana, A.; Sasso, F. P., Thompson, J. B. J, Guggenheim, S., Eds.; MSA, 2002; Vol. 46, pp 1−97.
(29) Reed, D. T.; Scott, D. D.; Weiner, M. F., *Gamma and alpha radiation levels in a basalt high-level waste repository: potential impact on container corrosion and packing properties. In Coupled Processes Associated with Nuclear Waste Repositories:*, Tsang, C., Ed.; Academic Press, Orlando, 1987, pp 325−338.
(30) Godon, N. Technical Report CEA (Comissariat à l'Energie Atomique) RT DTCD/2004/06 **2004**.
(31) Farnan, I.; Cho, H.; Weber, W. J. Quantification of actinide α-radiation damage in minerals and ceramics. *Nature* **2007**, *445*, 190–193.

ES800766B